# XV. NEUROLOGY*


| | | |
|---|---|---|
| Dr. L. Stark | C. A. Finnila | Julia H. Redhead |
| Dr. H. T. Hermann | Jeannette S. Hargroves | Helen E. Rhodes |
| Dr. Y. Okabe | L. A. Hoffman | A. A. Sandberg |
| Dr. G. Vossius | W. Kipiniak | G. Sever |
| Dr. G. Zames | H. Levy | L. A. M. Verbeek |
| Elise Audet | M. SiK Oh | P. A. Willis |
| A. W. England | R. C. Payne | L. R. Young |


## A. TRANSFER FUNCTION OF A BIOLOGICAL PHOTORECEPTOR

A full description of the function of a sensory organ, or sensory element, should include definition of the limits of signal transfer. This can be done if the stimulating energy is monitored and, at the same time, the nervous impulses emanating from the sensory receptor are detected and studied. It is believed that the signal that represents the input stimulus, and is transmitted to other centers of the central nervous system, is the average frequency of these nerve impulses. By correlating the instantaneous values of the stimulus and the nerve impulse signal, it is possible to make a rigorous statement regarding the transfer characteristics of the sensory receptor. The task, then, is to find the equation (generally an integro-differential equation) that characterizes the functional relationship between input and output (1-4).

To explore the problem, we have chosen to study the photosensitive tail ganglion of Cambarus Astacus, the common crayfish (5-8). Behavioral and reflex studies have demonstrated a physiological role for the receptor (9, 10).

Figure XV-1 shows the neuroanatomical structure as drawn by Retzius. The terminal abdominal ganglion, a translucent neuropil of 2-mm diameter receives fibers of several sensory modes from the uropods (7, 8). A small number of neurones, approximately 10, transduces photic energy. Lack of apparent spatial orginization in its structure, absence of lens, and sluggishness of behavioral response suggest that the ganglion serves to detect levels of background illumination only.

Through a window in the ventral abdominal exoskeleton, gross electrodes were applied to the ventral nerve cord. The animal was kept in a humidity and temperature-controlled environment (100 per cent saturation, 19° ± 0.5°C).

An electronically controlled light source was used to generate transient steps, as well as sinusoidal variations of light (11). Relatively small light fluctuations in a darkened environment permitted small-signal linearization.

The nerve impulses were averaged over a time period (Time constant = 0.24 sec) that was long with respect to pulse intervals, but short with respect to the response


*This research is supported in part by the U.S. Public Health Service (B-3055, B-3090); the Office of Naval Research (Nonr-609(39)); the Air Force (AF33(616)-7282); and the Army Chemical Corps (DA-18-108-405-Cml-942).

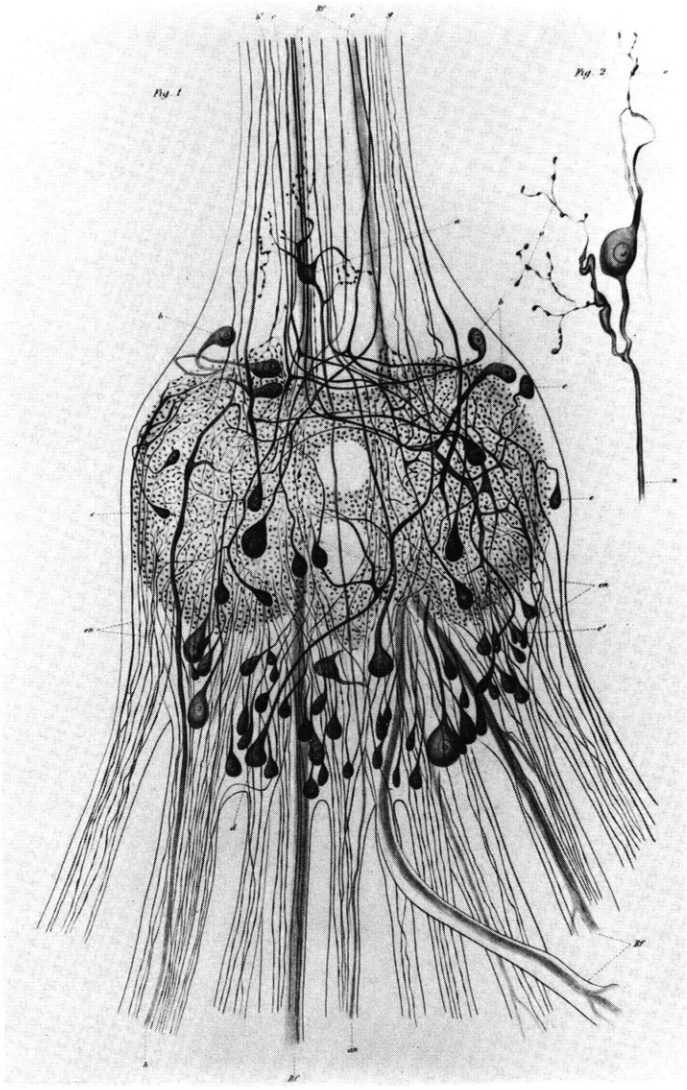

Fig. XV-1. Neuroanatomical structure of the crayfish's 6$^{th}$ abdominal ganglion (After Retzius).

frequency of the receptor. A combination of operational amplifiers, pulse-shaping circuits, and lowpass filters carried out the averaging. An amplitude window screened from the averaging process any pulses with heights greater or smaller than the medium-sized pulses carrying the light-energy information (12).

A response of the photoganglion to a sinusoidal stimulus is shown in Fig. XV-2. The noise comes in part from random groupings of pulses from different fibers. Harmonic distortion was minimized by the small-signal experimental conditions, but still is apparent here. The mean amplitude of response over a number of cycles and the mean-phase relationship between stimulus and response were determined from such a

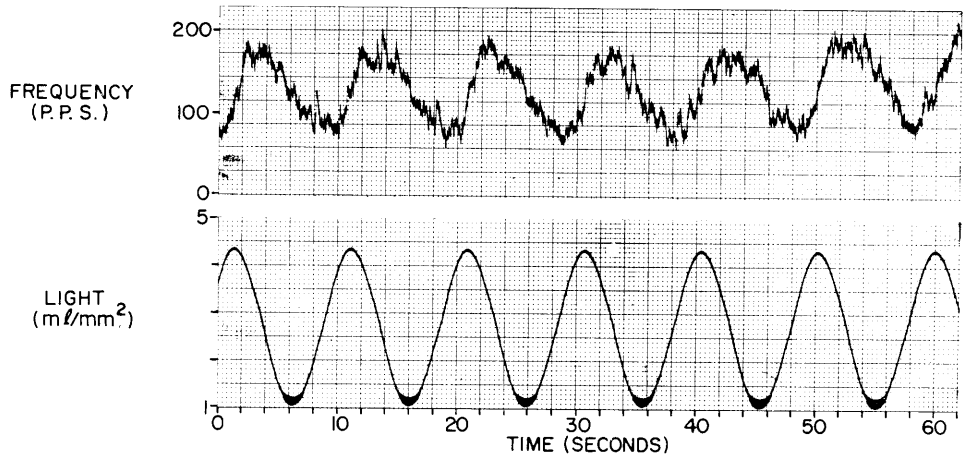


Fig. XV-2. Response of a photoreceptor to sinusoidal light changes. Note that harmonic distortion is minimized by small-signal approach. The 0.01-cps input produces an output with amplitude of ± 70 pps, a mean of 130 pps, and a phase lag of 22°.

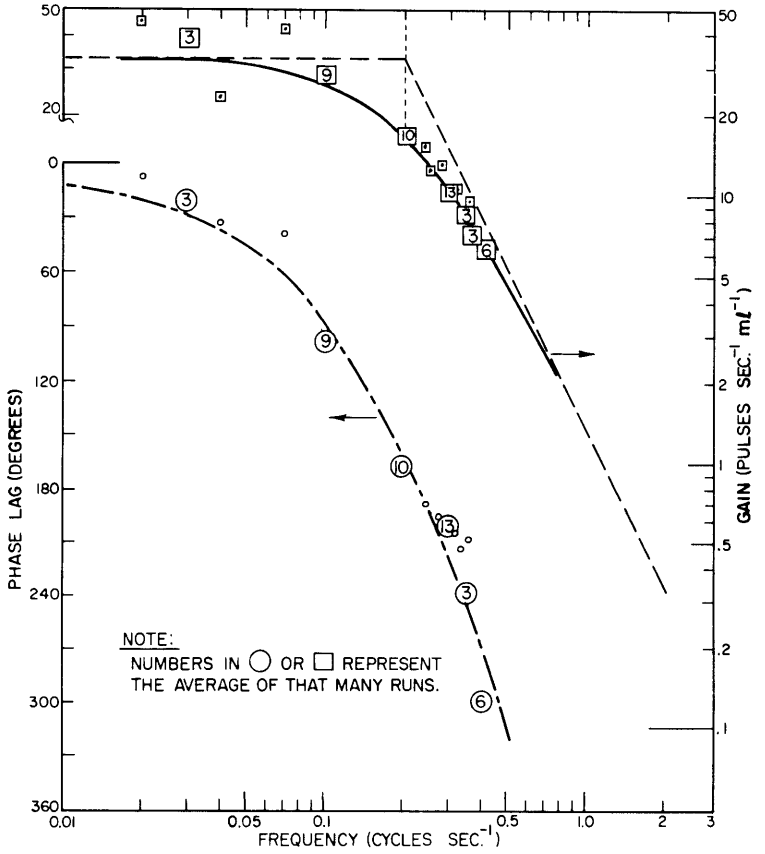


Fig. XV-3. Bode plot of photosensitive ganglion response. The solid curve represents the theoretical behavior of a system described by the transfer function. The dashed lines are asymptotes showing the break frequency and attenuation slope more clearly. The points are experimental.

recording. The parameter triplet: gain, phase, and frequency completely specifies a linear system.

The frequency response of the photosensitive ganglion was obtained by means of a series of experiments at different driving frequencies. Note in Fig. XV-3 the static or dc gain, the absence of adaptation, the break frequency, the attenuation slope, and the large phase lag, composed of both minimum and nonminimum elements. A transfer function

$$G(s) = 32 \frac{e^{-s}}{(1+1.2s)^2} \text{ p sec}^{-1} \text{ mlum}^{-1}$$

in Laplace operator (s) notation can be quantitatively derived from this graphic display of system behavior (3). It is somewhat more convenient than the equivalent integro-differential equation,

$$32\, L(t-1) = 1.44 \frac{d^2P}{dt^2} + 2.4 \frac{dP}{dt} + 1P$$

where L is the light flux in millilumens, P is the pulses per second, and T is the time in seconds.

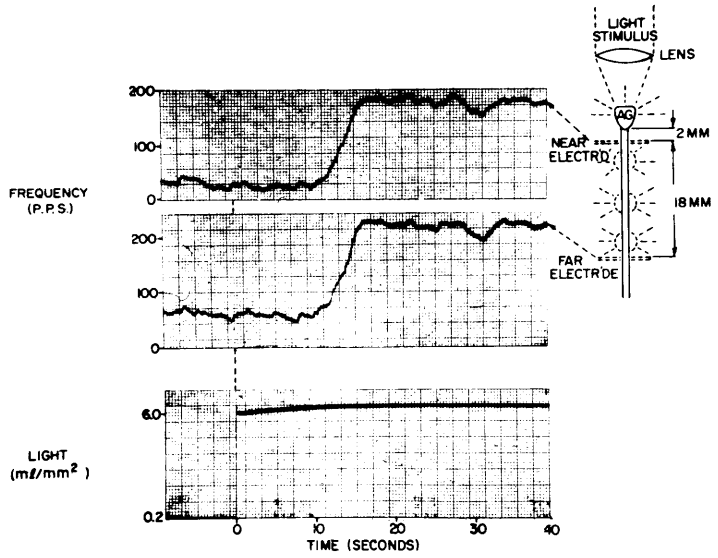


Fig. XV-4. Transient experiment. The lack of contribution of nerve conduction time to the nonminimum phase element (time delay) is shown. Thus, processes in the photosensitive ganglion are responsible for this operator. Conduction velocity is approximately 4 m/sec. It is interesting to note that details of the response are preserved over the 18-mm conduction path through 3 abdominal ganglia. This step of light was rather large, violating completely the theory of small-perturbation analysis. Apparent damping is inversely proportional to forcing-function amplitude.

The time-delay operator that accounts for the nonminimum phase lag results not from nerve conduction time, but rather from processes in the photosensitive ganglion, as reference to Fig. XV-4 demonstrates. Further investigation of nonlinearities is proceeding; it can be seen from the large-signal step experiments that the law of superposition does not hold.

L. Stark, H. T. Hermann

References

1. J. W. S. Pringle and V. J. Wilson, The response of a sense organ to a harmonic stimulus, J. Exptl. Biol. 29, 220-234 (1952).

2. L. Stark and P. M. Sherman, A servoanalytic study of the consensual pupil reflex to light, J. Neurophysiol. 20, 17-26 (1957).

3. L. Stark, Transfer Function of a Biological Photoreceptor, WADC Technical Report 59-311, August 1959.

4. H. K. Hartline, A quantitative and descriptive study of the electrical response to illumination of the anthropod eye, Am. J. Physiol. 83, 466-483 (1928).

5. C. L. Prosser, Action potentials in the nervous system of the crayfish. II. Responses to illumination of the eye and caudal ganglion, J. Cell Comp. Physiol. 4, 363-377 (1934).

6. J. H. Welsh, The caudal photoreceptor and responses of the crayfish to light, J. Cell Comp. Physiol. 4, 378 (1934).

7. D. Kennedy, Responses from the crayfish caudal photoreceptor, Am. J. Opthalmol. 11, 19-26 (1958).

8. C. A. G. Wiersma, S. H. Ripley, and E. Christensen, The central representation of sensory stimulation in the crayfish, J. Cell Comp. Physiol. 46, 307-326 (1955).

9. B. Kropp and E. V. Enzmann, Photic stimulation and leg movements in the crayfish, J. Gen. Physiol. 16, 905 (1933).

10. H. T. Hermann and L. Stark, Random walk response of the crayfish, Quarterly Progress Report No. 61, Research Laboratory of Electronics, M.I.T., April 15, 1961, pp. 230-234.

11. L. Stark, Stability, oscillations, and noise in the human pupil servomechanism, Proc. IRE 47, 1925-1939 (1959).

12. H. T. Hermann, L. Stark, and P. A. Willis, Instrumentation for study of nerve impulse codes (Technical Note, Electronic Systems Laboratory, M.I.T., forthcoming).

## B. ANALYSIS OF PUPIL RESPONSE AND NOISE

In an attempt to quantify the pupillary frequency response characteristics (1) we were led to a study of the interaction of the signal and the large amount of biological noise present (2). Several decades of frequencies of interest were studied, with allowances being made for sampling epoch, sampling rate, and bandpass filtering as shown in Table XV-1. Figures XV-5, XV-6, XV-7 show experimental runs of noise alone (that is, with a dc light level) and of noise mixed

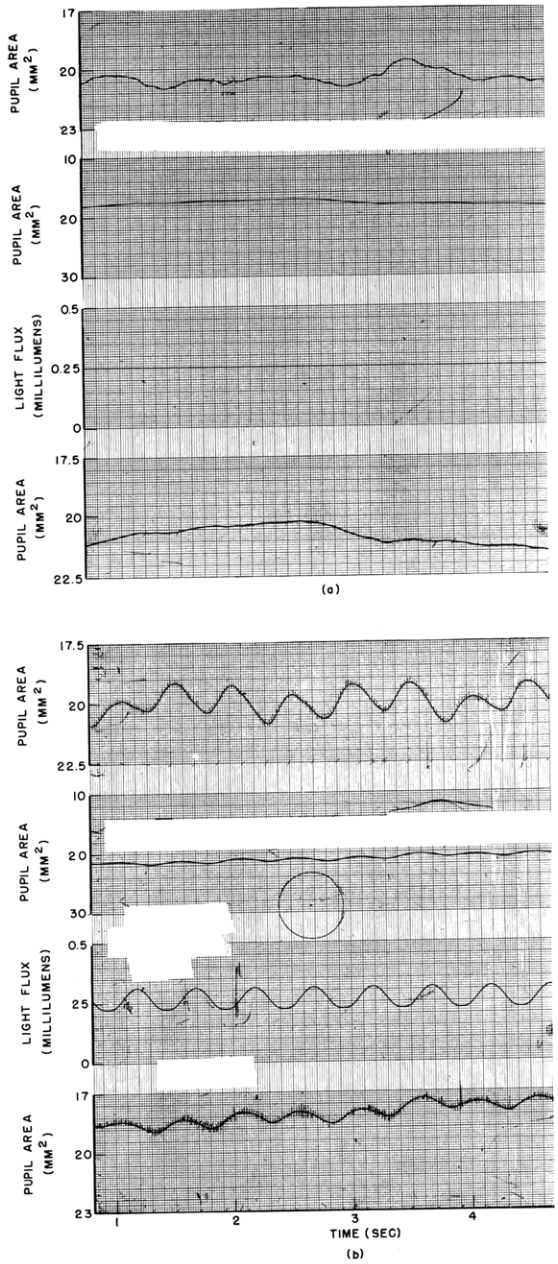


Fig. XV-5. (a) Pupil noise at 2.0 cps. First and second traces: Same as (b). Third trace: Light flux onto retina held constant. Fourth trace: Pupil area at high amplification, showing random fluctuations that are not coherent with the dc input signal and are considered as noise.

(b) Pupil response to signal plus pupil noise at 2.0 cps. First trace: Pupil area at even higher amplification in trace 4(a). The signal has been passed through a bandpass filter with 24 db per octave slopes and break frequencies as shown in Table XV-1. Second trace: Pupil area at low amplification, which is used to keep a careful record of the average pupil area. Third trace: Fluctuations of light flux input in open-loop operating conditions. Fourth trace: Pupil area at high amplifications, showing response of the pupil to fluctuations of light intensity superimposed on noise or random fluctuations that are not coherent with the input signal.

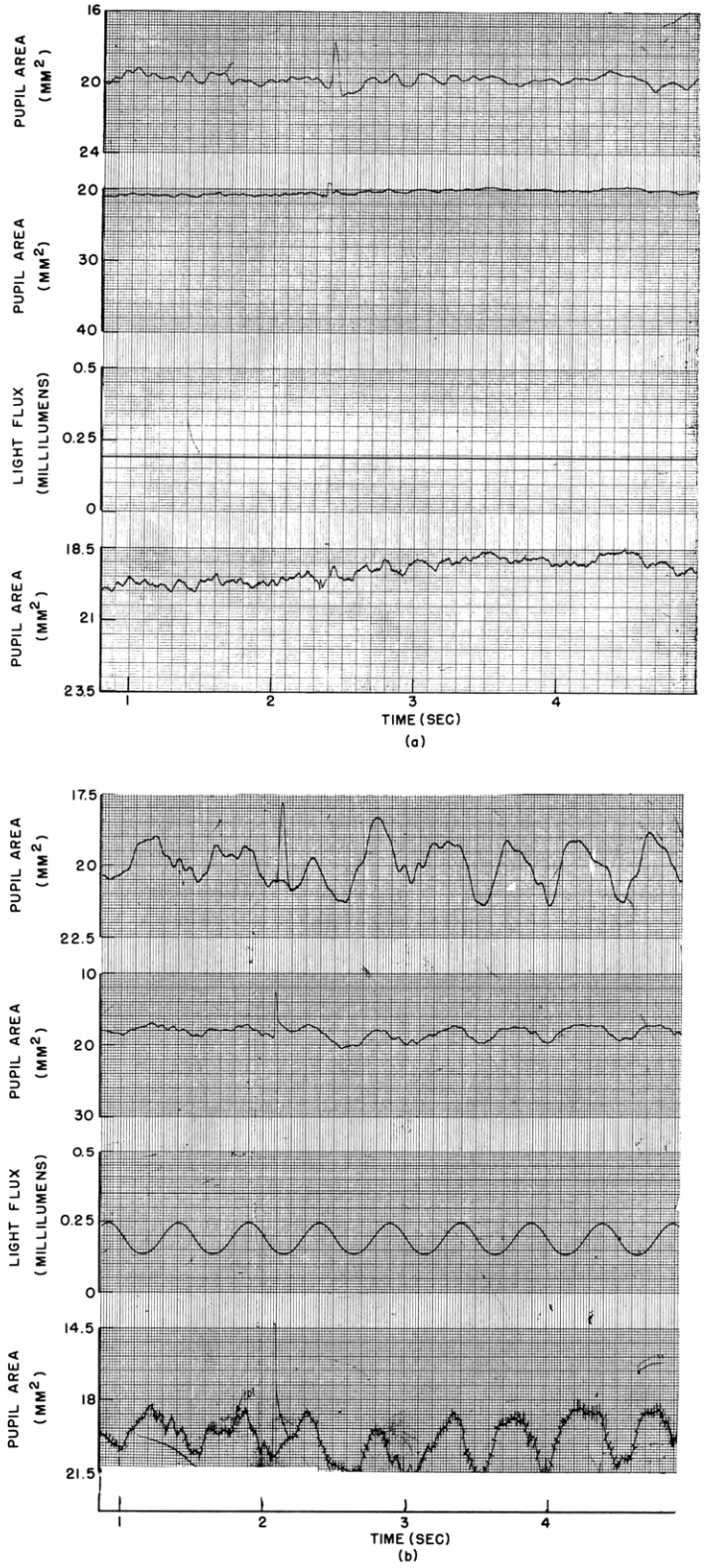


Fig. XV-6. (a) Pupil noise at 0.2 cps, showing same outputs and inputs as in Fig. XV-5a. (b) Pupil response to signal plus noise at 0.2 cps, showing same outputs and inputs as in Fig. XV-5b.

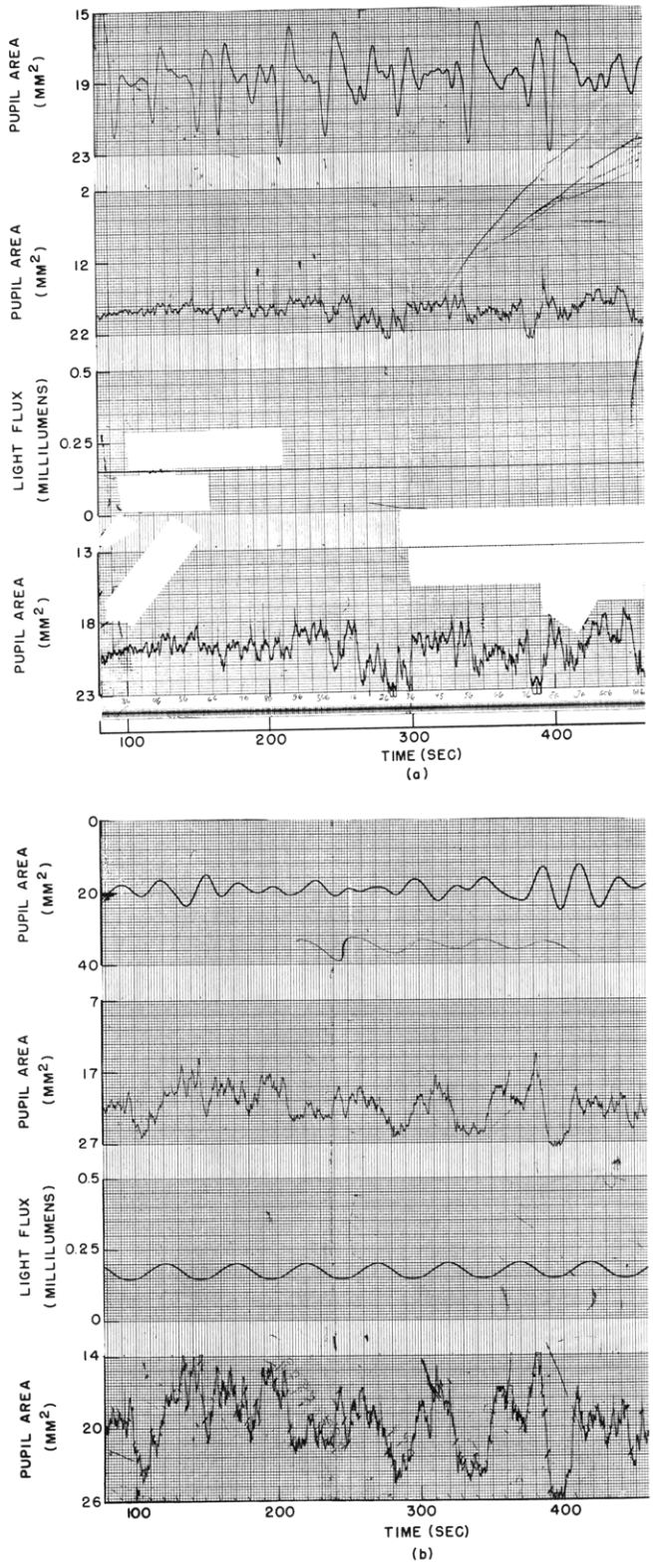


Fig. XV-7. (a) Pupil noise at 0.02 cps, showing same outputs and inputs as in Fig. XV-5a. (b) Pupil response to signal plus noise at 0.02 cps, showing same outputs and inputs as in Fig. XV-5b.

with signal. The data were hand-digitalized, and the subsequent punched cards were processed at the Yale Computing Center with the help and advice of Dr. Morris Davis.

Table XV-1.

| Cycles | 0.02 cps | 0.2 cps | 2.0 cps |
|---|---|---|---|
| Paper Speed | 0.5 mm/sec | 5 mm/sec | 50 mm/sec |
| Filter Settings | 0.003-0.12 cps | 0.03-1.2 cps | 0.3-12 cps |
| Time of Run | 33.33 min | 3.33 min | 20 sec |

Autocorrelation functions were computed as shown in Figs. XV-8 and XV-9. These figures contrast unfiltered and filtered data, showing the strong influence of

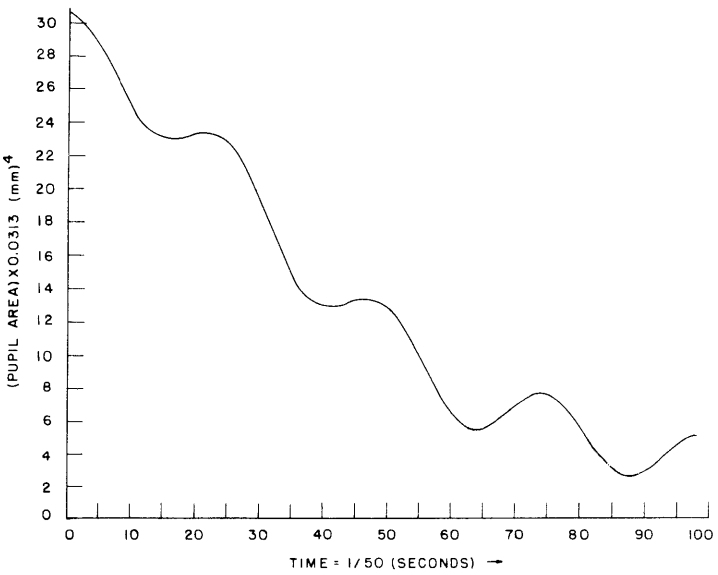


Fig. XV-8. Autocorrelation function (pupil area)$^2$ versus delay time for 2.0-cps sine input unfiltered response. The pupil area is calculated in mm$^2$; then it is squared and multiplied by the constant 0.0313 to give quantities in mm$^4$ that are plotted on the graph. Time, shown on the abscissa, is marked in seconds and multiplied by the constant 1/50.

frequencies outside of the immediate range of interest and, in fact, outside of reasonable sampling measurements. It is of interest to restudy the filtered and unfiltered data in Figs. XV-5, XV-6, and XV-7 with these autocorrelation functions in mind.

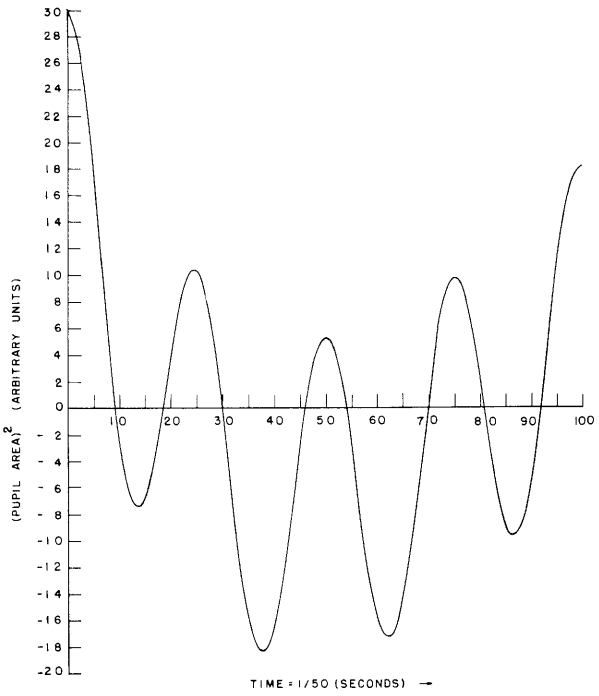


Fig. XV-9. Autocorrelation function (pupil area)$^2$ versus delay time for 2.0-cps sine input filtered response. The (pupil area)$^2$ is graphed in arbitrary units. Time, as shown on the abscissa, is marked in seconds and multiplied by the constant 1/50.

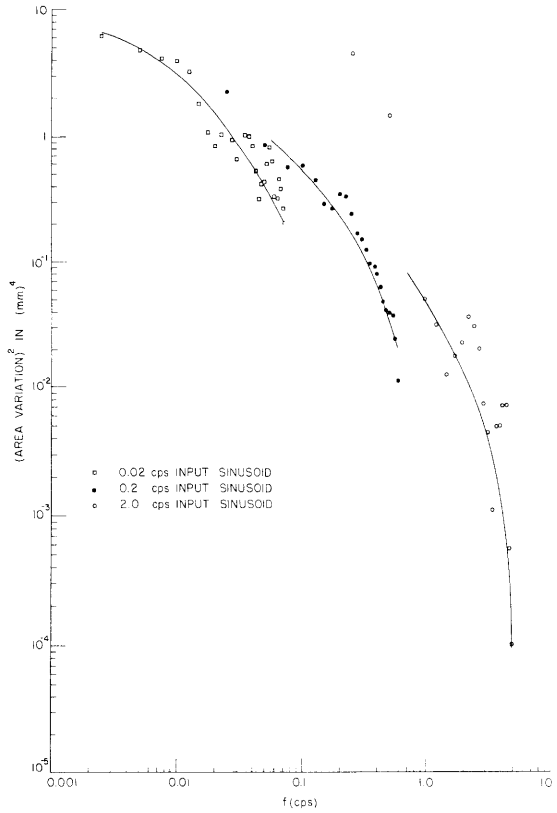


Fig. XV-10. Power spectrum of noise over frequency range 0-4.5 cps, constructed from data runs at speeds corresponding to response frequency speeds for 0.02, 0.2, and 2.0 cps. Variation in (pupil area)$^2$ in (mm$^4$) versus frequency (cps).

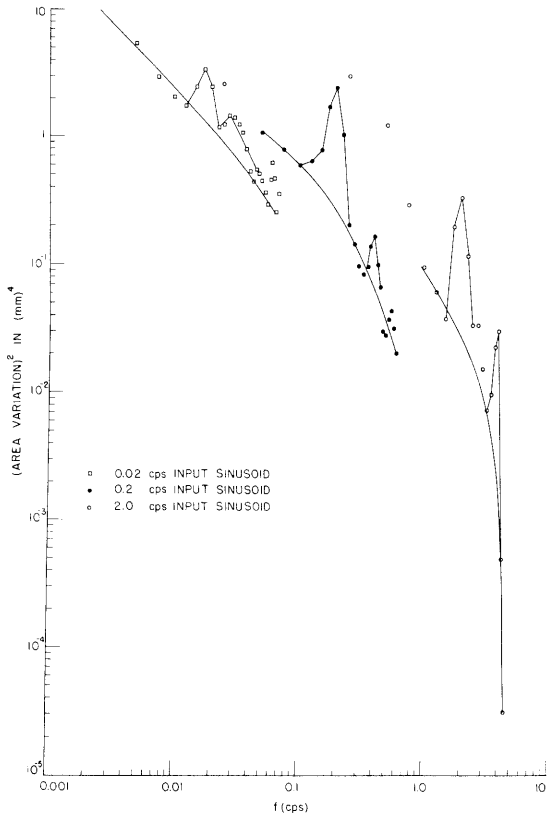


Fig. XV-11. Power spectrum of input sinusoidal responses of 0.02, 0.2, and 2.0 cps, taken from three different data runs. Variation in $(\text{pupil area})^2$ in $(\text{mm}^4)$ versus frequency (cps).

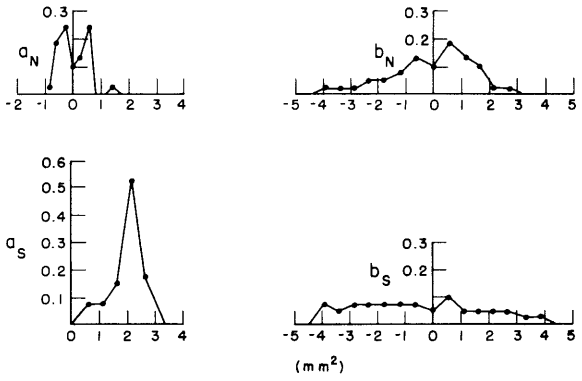


Fig. XV-12. Normalized probabilities of Fourier coefficients. These curves show the distribution of Fourier coefficients for the two experimental conditions shown in Fig. XV-5a and 5b (2 cps). Curves $a_n$ and $b_n$ show alpha and beta Fourier coefficients for the noise case; curves $a_s$ and $b_s$ show alpha and beta Fourier coefficients for the signal plus noise case. The ordinates are normalized, and the abscissa represents the area in $\text{mm}^2$.

Power spectra were computed from the autocorrelation functions and the additive effect of signal on the noise can be noted by comparing Fig. XV-10 (noise alone) with Fig. XV-11 (noise plus signal). These studies extend and confirm earlier published work on pupil noise (2).

The Fourier coefficients of the signal response were computed cycle by cycle (for

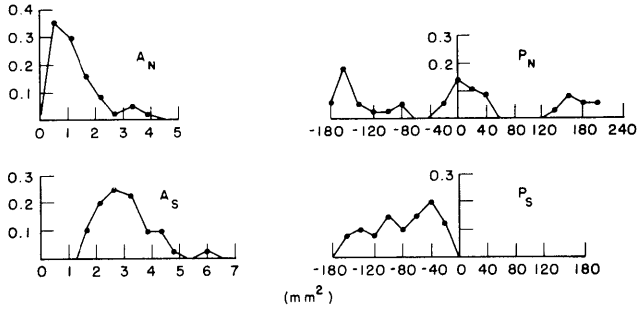


Fig. XV-13. Normalized probabilities of amplitude and phase coefficients. These curves show the distribution of amplitude and phase coefficients for the two experimental conditions shown in Fig. XV-5a and 5b (2 cps). Curves $A_N$ and $P_N$ show amplitude and phase coefficients for the noise case; $A_S$ and $P_S$ show coefficients for the signal plus noise case. The ordinates are normalized and the abscissas represent area in $mm^2$ for the amplitudes, and in degrees for the phase.

40 cycles) and their statistical distribution was studied. Figure XV-12 shows this distribution of the alpha and beta coefficients for a noise plus signal run and for a noise run (in which, in fact, no signal existed). It can be seen that there is an approximate Gaussian distribution (considering the small population sample of only 40), and that the signal clearly shifts the alpha coefficient mean, as would be expected. Figure XV-13 shows the distribution of the amplitude and phase characteristics of the same data. The amplitude coefficients are still quasi-Gaussian, and shifted upward by the signal, as expected. The phase coefficients for the noise alone show a peculiar and interesting distribution which was predicted from a mathematical study by Mr. Frank Kuhl under the direction of Professor P. M. Schultheiss, of Yale University (3). With signal added, the phase coefficients show an agglomeration about a phase lag of 300°, as expected from earlier studies (4).

The experimental results, in general, confirm the validity of treating the pupillary response as a signal additive to Gaussian pupillary noise.

L. Stark, F. Kuhl

(References on following page)

References

1. L. Stark, Stability, oscillations and noise in the human pupil servomechanism, Proc. IRE 47, 1925 (1959).

2. L. Stark, F. W. Campbell, and J. Atwood, Pupil unrest: An example of noise in a biological servomechanism, Nature 182, 857 (1958).

3. F. J. Kuhl, Methods of Analyzing the Response of a Neurological Servomechanism, Technical Report, Electrical Engineering and Neurology Departments, Yale University, May 1959.

4. L. Stark and P. Sherman, A servoanalytic study of consensual pupil reflex to light, J. Neurophysiol. 20, 17 (1957).

## C. FURTHER STUDIES ON THE APPLICATION OF COMPUTER ANALYSIS TO MEASUREMENT OF MOVEMENT DYNAMIC CHARACTERISTICS

In previous studies (1, 2) the general dynamic characteristics of the human motor coordination system were presented, and recently a description has been given of the

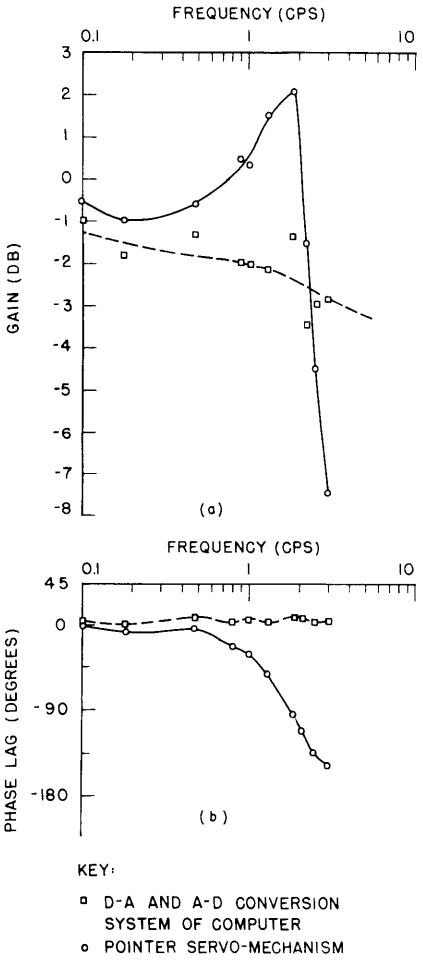


Fig. XV-14. Calibration of RW-300 computer and its D-A and A-D conversion system, and the pointer servomechanism. The ordinates represent gain in decibels (a), and phase lag in degrees (b). The abscissa represents frequency in cycles per second.

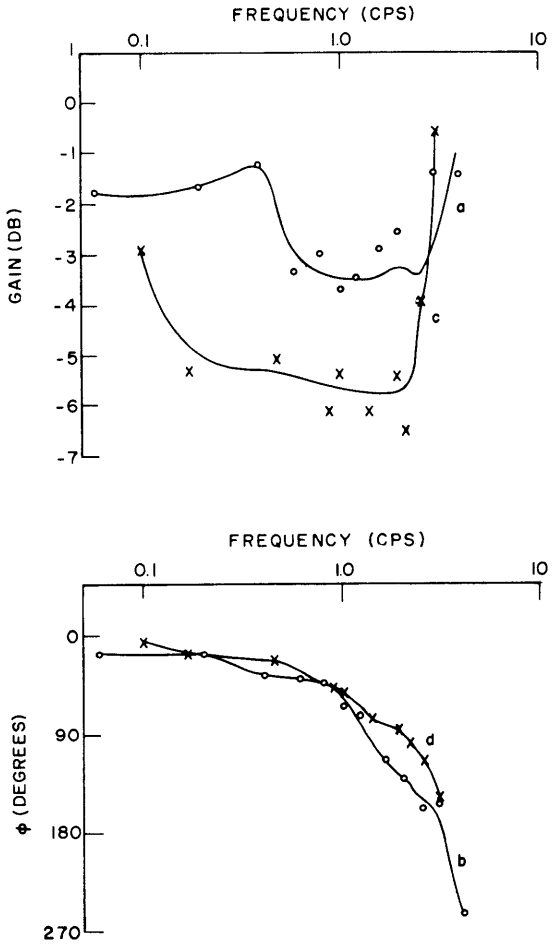


Fig. XV-15. Bode plot showing wrist-rotation response of a normal subject, Y.O. (Scales are the same as in Fig. XV-14.) Key: (a) and (b), three-frequency and pencil and ruler analysis; (c) and (d), ten-frequency and computer analysis.

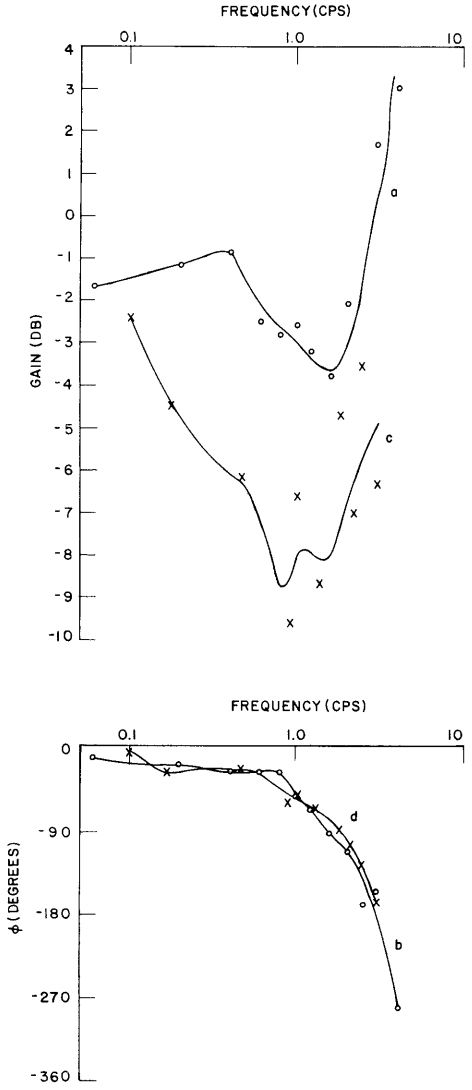


Fig. XV-16. Bode plot showing finger response of normal subject, Y.O. (Scales and key same as in Fig. XV-15.)

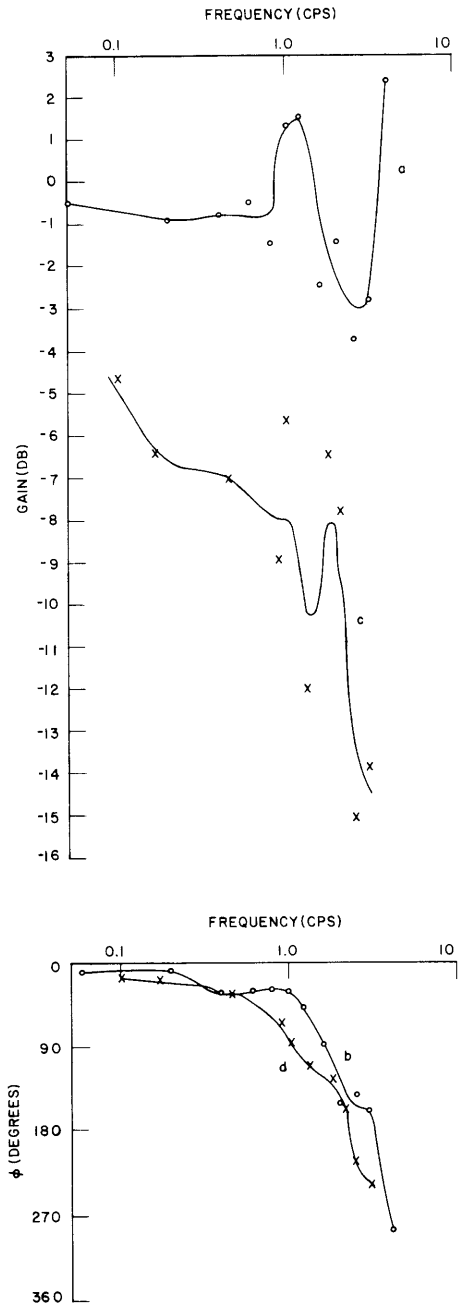


Fig. XV-17. Bode plot showing finger response of normal subject, H.R. (Scales and key same as in Fig. XV-15.)

rise of an on-line digital computer for these experiments (3). This report compares different operating conditions, analysis methods, neuromuscular movement systems, and subjects, in order to ascertain important factors in our descriptions.

Calibrations were performed on the computer and its D-A and A-D conversion system, and on the pointer servomechanism as shown in Fig. XV-14.

These effects were accounted for before plotting the experimental results shown in the other figures.

Wrist rotation of an experienced subject (Y.O.) was studied by using groups of three superimposed frequencies as the complex unpredictable input and 10 superimposed frequencies. The three-frequency experiments were analyzed by pencil and ruler, and the ten-frequency experiments by computer. The results are compared in Fig. XV-15. Here we see that the gain is markedly reduced in the ten-frequency experiment. This may be due to one of two causes; the subject's performance may be so spread over the entire power distribution of the input that he responds less at each individual frequency, or the pencil-and-ruler analysis may emphasize portions of the recording in which the response shows a relatively high gain. The phase curves are almost identical.

When we compare a different neurological movement, extension and flexion of the forefinger as shown in Fig. XV-16, we find that the gain curves closely resemble the wrist rotation curves. This suggests that the characteristics and the underlying complex impedances that shape these curves are dominated by the neurological, rather than by the mechanical elements. Again, we see the effect of the larger number of frequencies and/or computer analysis in diminishing the gain. The phase curves are identical, as before, and show no significant differences between each other and with those of Fig. XV-15.

In Fig. XV-17 are shown analogous experiments on another experienced subject (H.R.) to show the variability from one subject to the next. Here we also see more variability from condition to condition. The same attenuation of gain with the ten-frequency input is seen, however.

Further experiments are underway to control and evaluate the various factors whose interplay may complicate the interpretation of these Bode curves.

Y. Okabe, Helen E. Rhodes, L. Stark, P. A. Willis

## References

1. L. Stark, M. Iida, and P. A. Willis, Dynamic characteristics of the motor coordination system in man, Biophys. J. 1, pp. 279-300 (1961).

2. L. Stark, M. Iida, and P. Willis, Dynamic characteristics of motor coordination, Quarterly Progress Report No. 60, Research Laboratory of Electronics, M.I.T., Jan. 15, 1961, pp. 231-233.

3. Y. Okabe, R. C. Payne, H. Rhodes, L. Stark, and P. A. Willis, Use of on-line digital computer for measurement of a neurological control system, Quarterly Progress Report No. 61, Research Laboratory of Electronics, M.I.T., April 15, 1961, pp. 219-222.

## D. A SIMPLE INSTRUMENT FOR MEASURING EYE MOVEMENTS

A simple device for measuring horizontal eye movements, which is similar to that of Richter (1), has been constructed. The method is based on differentiating the light reflected from the sclera (white) of the eye on either side of the iris and pupil. Figure XV-18a shows the arrangement of light sources and photocells as mounted on a pair of goggles worn by the human subject. Figure XV-18b shows how light is reflected

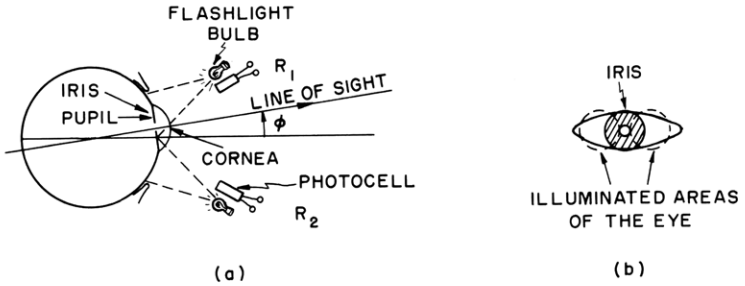


Fig. XV-18. (a) Light bulb and photocell arrangement.
(b) Front view of eye for $\phi = 0$.

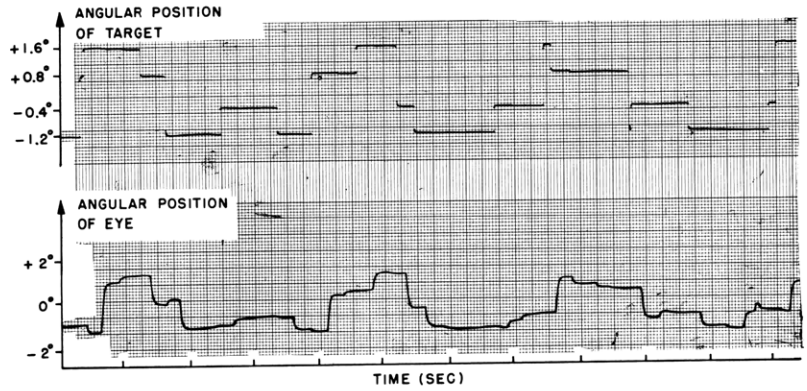


Fig. XV-19. Time-function record showing target movement and following eye movement.

from either side of the eye, and it is clear that the amount of sclera, and hence of reflected light, is a function of the angle of sight.

Figure XV-19 shows a typical record of human eye tracking of an unpredictable set of step sequences. Target position was produced by a spot on the face of a cathode-ray oscilloscope. An improved target generator is described in this report, as well as a

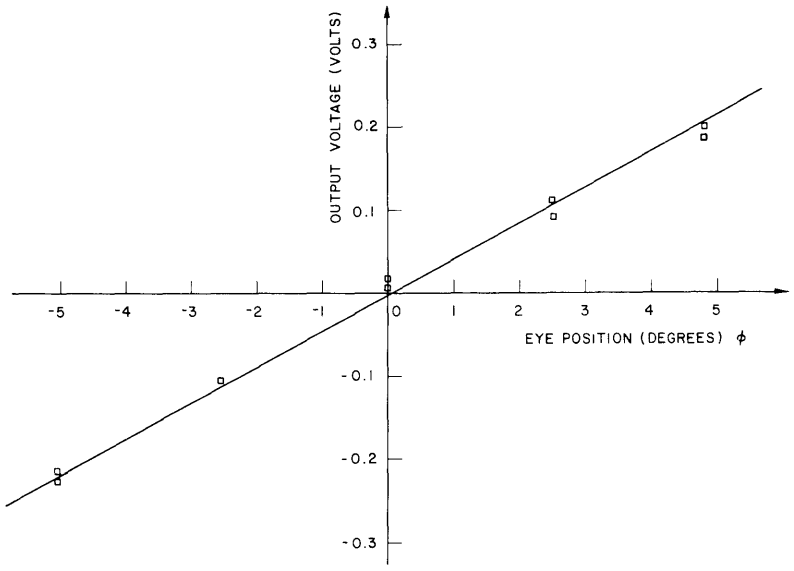


Fig. XV-20. Typical output voltage versus eye position.

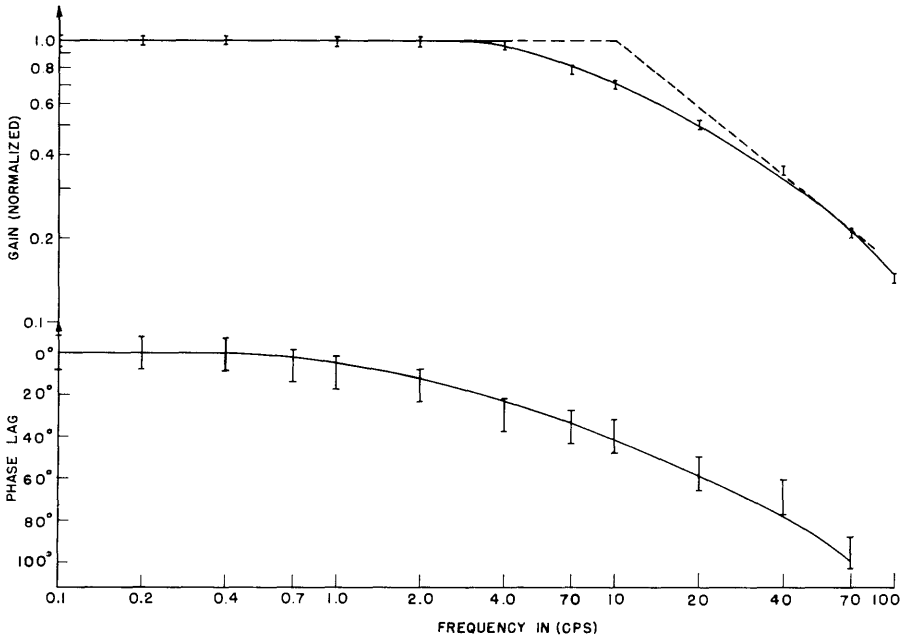


Fig. XV-21. Dynamic response of photocell.

number of experiments designed to study the mechanisms controlling eye movement.

Components used were flashlight bulbs (the type having a small lens integral with the envelope) and CdS photoresistor cells (Clairex CL-3). Figure XV-20 shows a linearity check (which is typical if care is taken in adjusting the goggles). Figure XV-21 shows the dynamic response of the photocell to high light intensity. Besides being slow, the frequency response is dependent upon light intensity; this suggests that another photocell type would be more satisfactory for study of high-velocity movements.

L. Stark, A. Sandberg

References

1. H. R. Richter and C. R. Pfaltz, À propos de l'électro-oculagraphie (Rapport préliminaire sur une nouvelle méthode), Confinia Neurologica, Vol. 16, No. 415, 1956.

## E. TARGET PROJECTION FOR TRACKING EXPERIMENTS

A convenient method for projecting a moving target has been developed and successfully used in our studies of the control of human eye movements. A specially designed

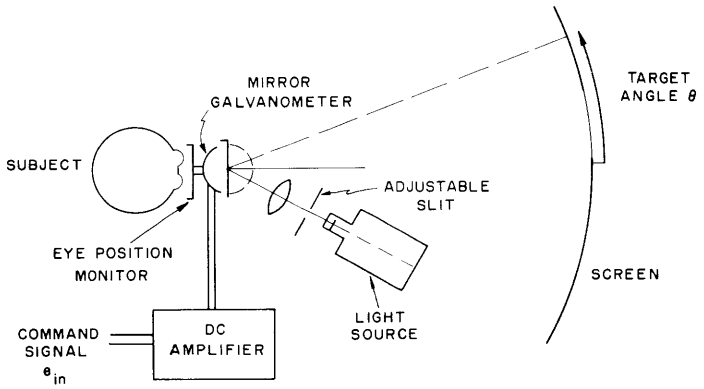


Fig. XV-22. Mirror galvanometer used in eye-movement studies.

mirror galvanometer, manufactured by the Sanborn Company and specified by Dr. H. T. Hermann, enables us to control the position of the projected target according to any function generated by our analog equipment. A block diagram of the apparatus as set up for eye-movement investigation is shown in Fig. XV-22.

The sensitivity of the system is 80 milliradians/volt with direct current, and its linear range is ±200 milliradians (±12°), as shown in Fig. XV-23. The sensitivity and range can obviously be increased at the expense of defocusing by increasing the screen-to-galvanometer distance.

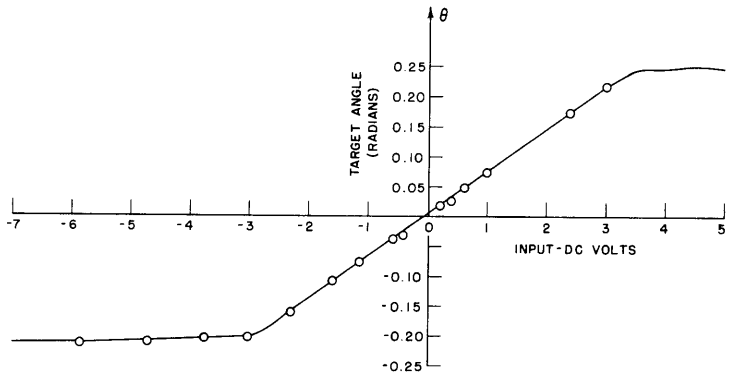


Fig. XV-23. Calibration of amplifier and galvanometer.

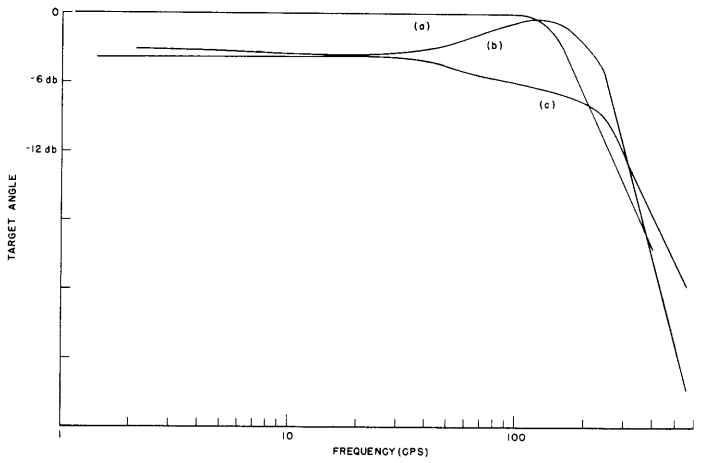


Fig. XV-24. Frequency response of mirror galvanometer. (a) Damping position No. 1 (critical). (b) Damping position No. 2 (underdamped). (c) Damping position No. 3 (overdamped). (Voltage input, 0.4 volt p-p.)

The special features of the galvanometer which make it suitable for tracking studies are its large mirror (0.7 cm × 4.0 cm) and considerable damping; the frequency response is found to be flat out to 100 cps. (See Fig. XV-24.)

L. R. Young

## F. PREDICTIVE CONTROL OF EYE MOVEMENTS

The exact nature of the multiloop control system governing eye tracking is still largely unknown, although two principal types of movement have long been distinguished (1).

The saccadic jump is characterized by its high velocity (this velocity, 60-300°/sec, is roughly proportional to total angle of movement), the inability to consciously control the velocity, pauses of at least 100 msec between successive saccades, and possible

absence of foveal vision during the saccadic movement. The magnitude and direction of the saccade is generally such as to correct for position error.

"Smooth pursuit" movements, on the other hand, are slow (less than 20°/sec), seem to be continuous, are not produced consciously, occur only when the eye is tracking a smoothly moving target, and seem to keep the target image stabilized with respect to the retina, rather than fixated (2).

These two movements are integrated in any tracking task as illustrated in Fig. XV-25. The important points to note are the initial time delay, the occurrence of saccades to

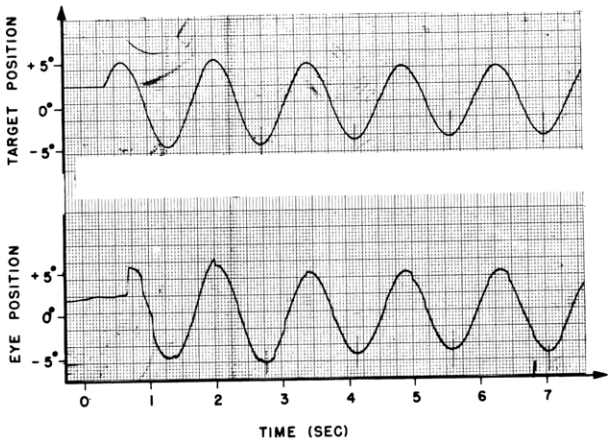


Fig. XV-25. A typical tracking record, showing reaction time, saccadic jumps, and smooth movements.

correct any appreciable error (often more prominent in the early portions of the task), and the smooth pursuit movements locking onto the target.

Previous dynamic descriptions of eye-tracking behavior have not been arrived at with sufficient control of important aspects of the input signal; in particular, unpredictable inputs have not been used to clarify different properties of the control system. We have contrasted the response to predictable and unpredictable steps, as well as simple and complex patterns of sinusoidal changes in target position. The sum of several sinusoids, in fact, forms a pattern which the subject cannot predict, as shown by Stark, Iida, and Willis (3).

The method of measuring the eye position involved detection of the difference in diffuse reflected light from the sclera (white) and iris, as described in Section XV-D. We restricted ourselves to horizontal movements on normal subjects who used binocular vision; only the left eye was monitored. Calibrations were performed and only those experiments with acceptable linearity of measurement before and after a run were retained.

The target was a fairly bright projected vertical slip, 0.5 cm × 6.0 cm, which stood out clearly in the darkened room. Its position was controlled by driving a mirror galvanometer, as described in Section XV-E. The light used for measurement of eye position was in the peripheral field and did not obscure target view or interfere subjectively with our experienced subjects.

Inputs could be generated by analog function generators or by the analog output of the RW-300 digital computer. A description of the on-line use of this computer, as well as the program for frequency analysis, has been given in a previous report (4).

1. Experimental Results

a. Latent Periods in Response to Unpredictable and Predictable Steps

In Fig. XV-26a is shown the response of the eye to a series of unpredictable step changes of position. The input function was constructed by summing square waves of different amplitude and non-low-harmonically related frequencies. It will be noted that the movements are saccadic in nature, except for some low-velocity drifting. Small saccadic movements to correct fixation error that is due either to drifting, to overshoot or undershoot can also be seen. These are similar to those observed under steady fixation conditions.

In Fig. XV-27a is shown a typical histogram of the distribution of time delays from a series of unpredictable steps of the type illustrated in Fig. XV-26a. It will be noted that there is a lower limit of response time of 150 msec and a median time delay of 200 msec (5). Most occurrences of time delays greater than 450 msec appear in response to the second of two target steps that appear in rapid succession. When the target position was a square wave of a given frequency, the latent period was reduced as the subject learned the pattern.

Often, the eye movement preceded the change of target position. Figure XV-26b through 26f shows the results from five square-wave experiments. At very low repetition rate prediction is minimal; whereas for square-wave frequencies around 0.4-1.0 cps a prediction is maximal. A prediction of 100 msec might well, after allowing for the time of actual movement of the eye, have the eye on target when the target appears; therefore we call predictions greater that 100 msec "over predictions." In these cases the prediction can be so great that the eye has a chance to see itself in error; it still may not correct itself, but rather await the expected change of target position.

With moderate repetition rates (0.4-1 cps) the pattern seems to be a rapid build-up of prediction up to the limit of overprediction, and then a drop back to small prediction or a time delay. At higher repetition rates (1.3-1.7 cps) there seems to be less significant prediction. Occasionally, an entire step may be missed as shown in Fig. XV-26d. An interesting phenomenon at still higher frequencies (around 2.0 cps) is the occurrence

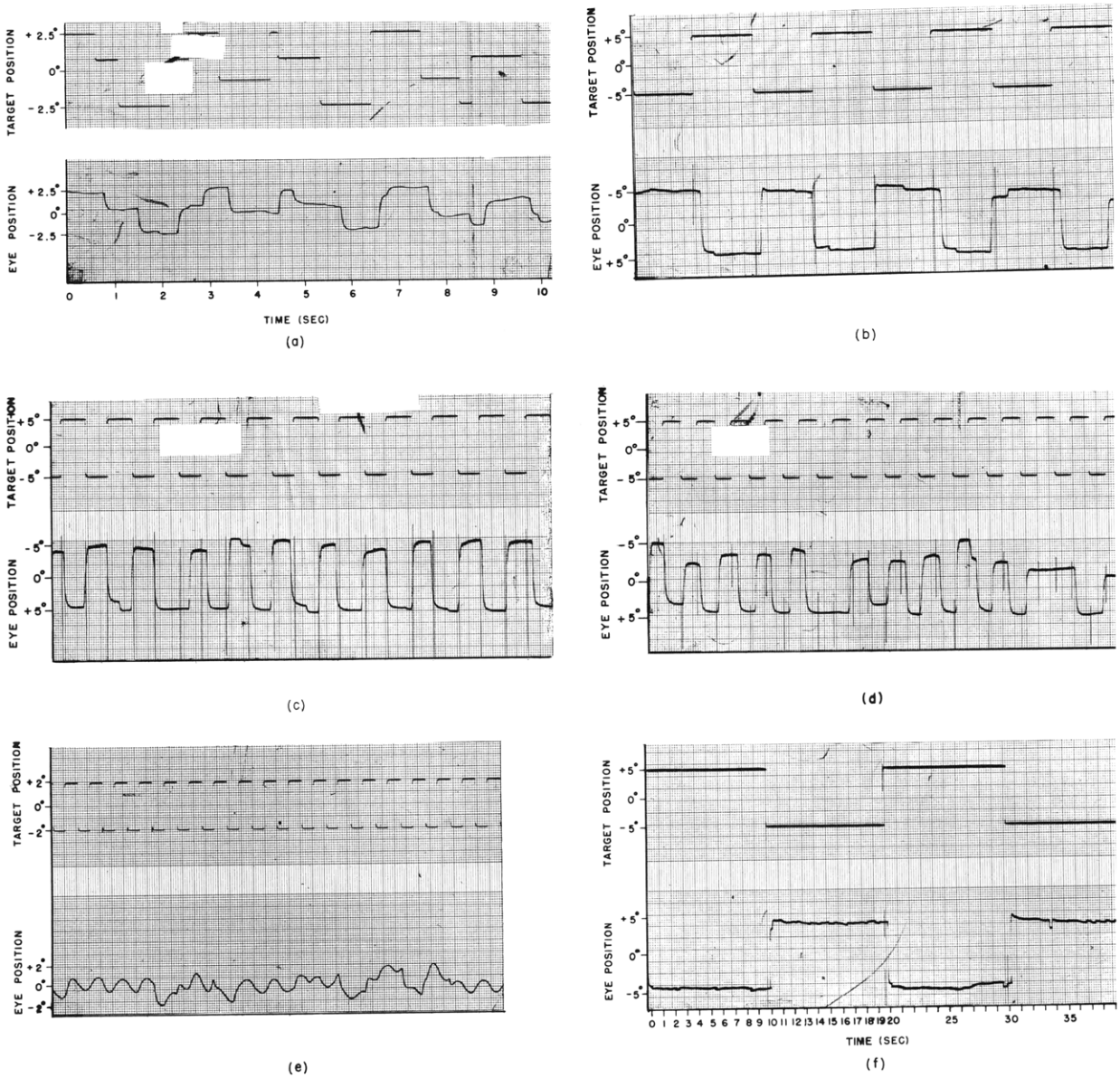


Fig. XV-26. Records of horizontal eye movements during tracking of random step and square-wave targets. (a) Eye movement during tracking of unpredictable steps. (b) Square wave, 0.4 cps. (c) Square wave, 1.0 cps. (d) Square wave, 1.5 cps. (e) Square wave, 2.0 cps. (f) Square wave, 0.05 cps.

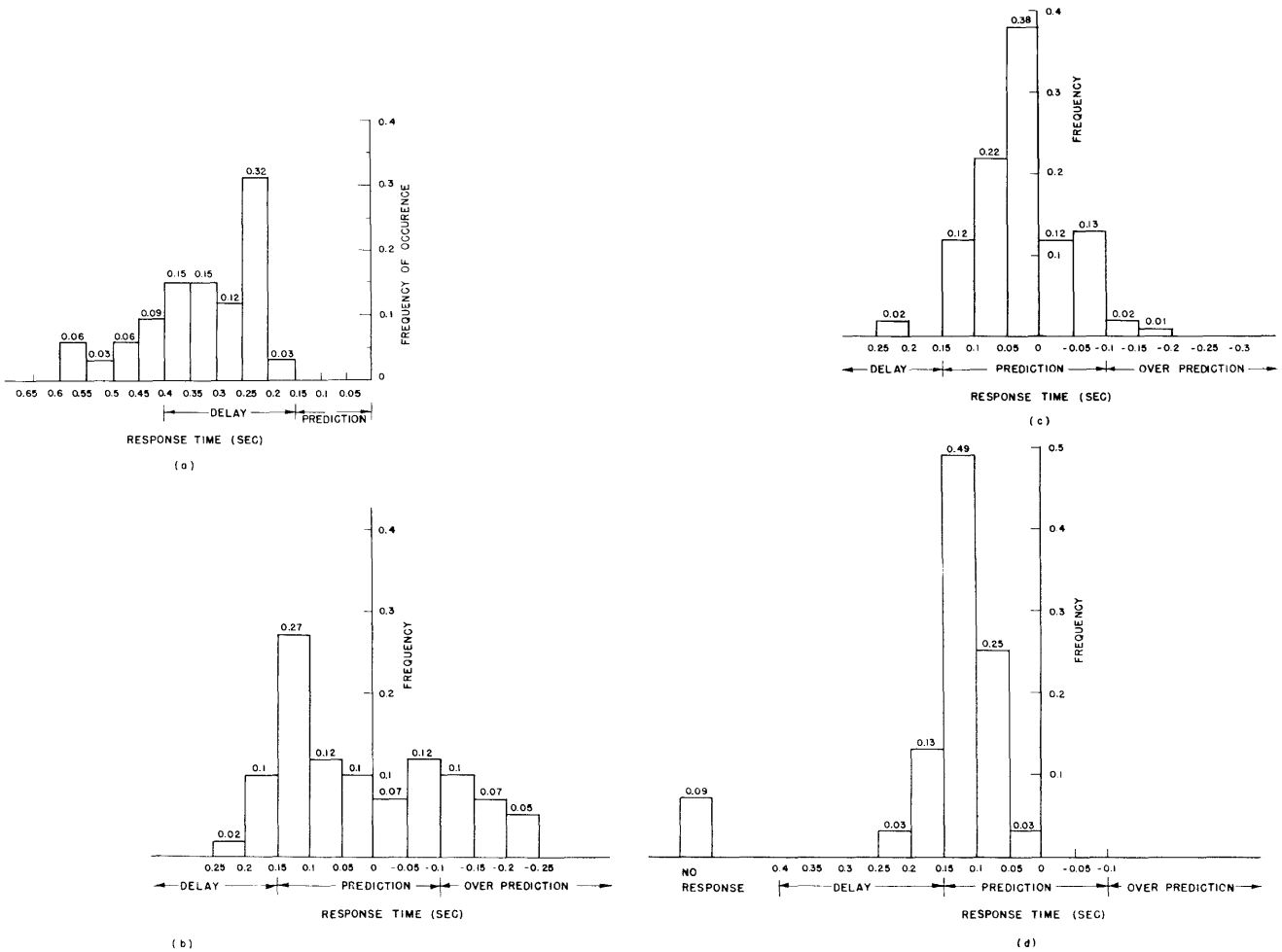


Fig. XV-27. Histograms of the frequency of occurrence of eye-movement response times for target motions of irregular steps and regular square waves of different frequencies. (a) Irregular steps. (b) Square waves, 0.4 cps. (c) Square waves, 1.0 cps. (d) Square waves, 1.5 cps.

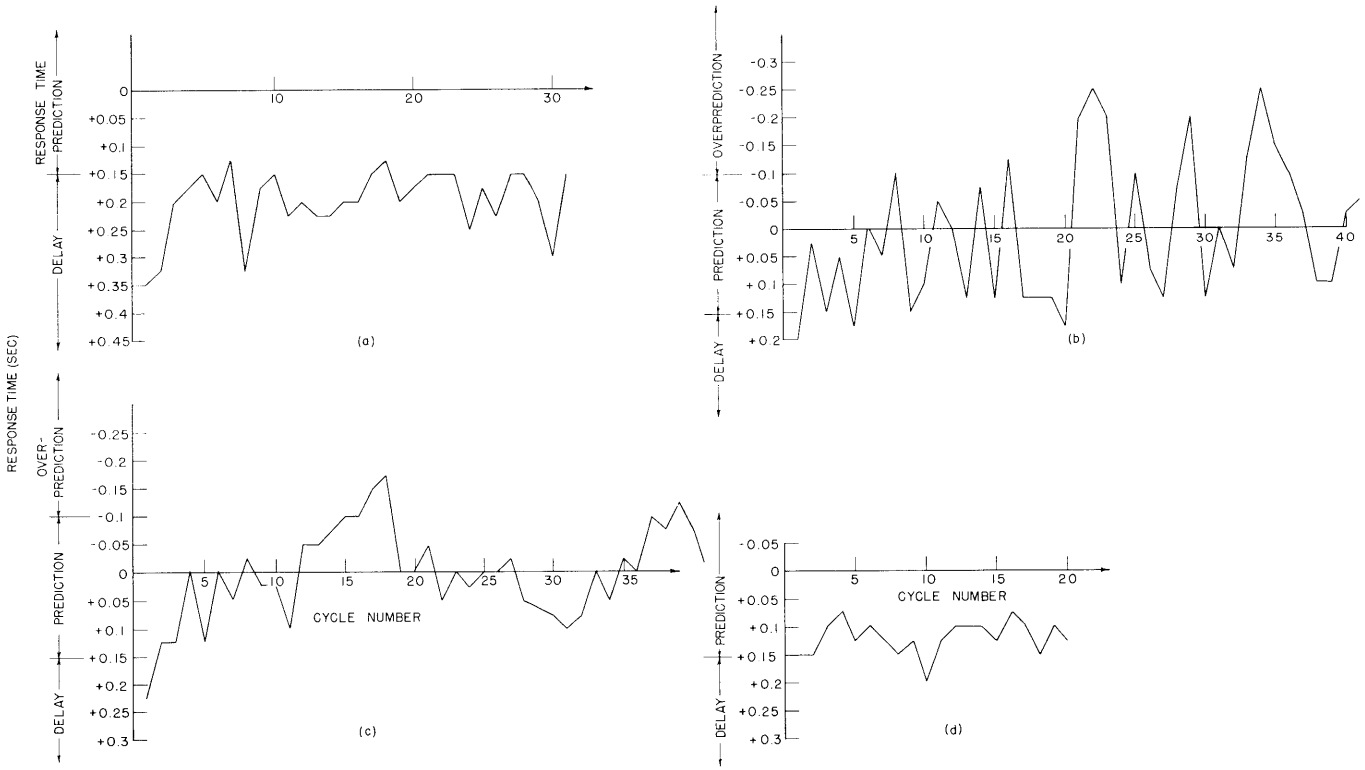


Fig. XV-28. Typical sequential patterns of time delays and predictions, starting with the onset of random step and square-wave target motions. (a) Sequential response times — irregular steps. (b) Square wave, 0.4 cps. (c) Square wave, 1.0 cps. (d) Sine wave, 1.5 cps.

of apparently continuous movements, rather than clear saccades. (See Fig. XV-26e.)

In Fig. XV-27c the histogram of time delays at a moderate repetition rate (1.0 cps) demonstrates the high frequency of prediction when the eye follows a regular pattern. Figure XV-27b is a histogram of time delays for a slow repetition rate (0.4 cps) and shows a greater occurrence of overprediction and delay. Figure XV-27d is a histogram showing the disappearance of overprediction and much of the prediction at 1.5 cps. These quantitative displays support the qualitative descriptions given above.

The sequential pattern of time delays and predictions is of interest and may be displayed as a plot of response times in sequential order, as in Fig. XV-28. Here, starting with the initial presentation of the square-wave pattern, the time delays, subsequent predictions, overpredictions, and reversions to time delays are exhibited. Figure XV-28c (1cps) shows the quick development of prediction but with minimum overprediction. Figure XV-28 exhibits the phenomenon of overprediction with occasional transitions back to predictions and delay.

After studying Fig. XV-28, the patterns of sequential response times, the reader should review Fig. XV-27, the histograms, and Fig. XV-26, the time functions, in order to better correlate these different displays of the prediction or learning process.

Figure XV-29 serves to summarize the variation of predictive behavior as a function of repetition rate. Here, the lack of prediction at very slow and very fast rates is

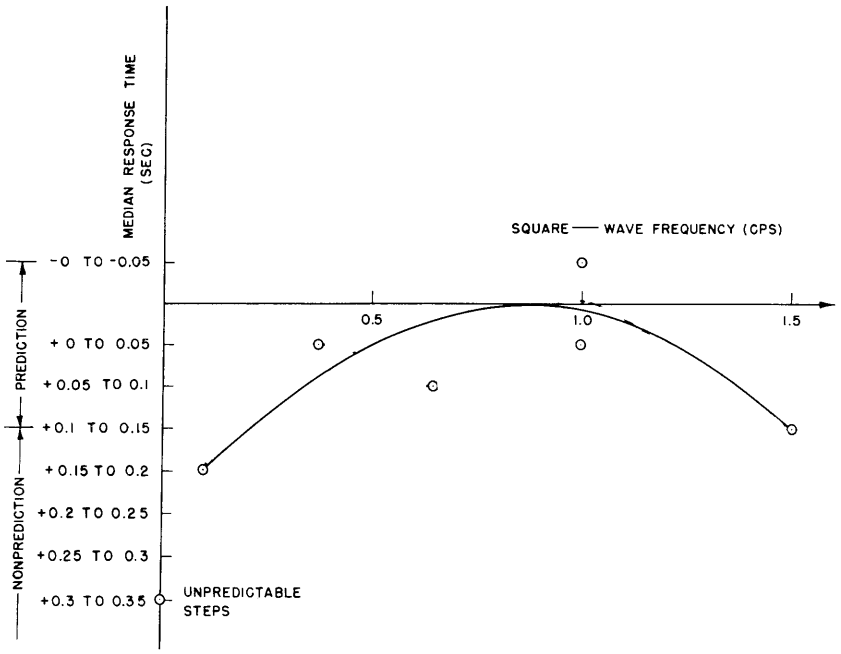


Fig. XV-29. Median response times in tracking target motion of unpredictable steps and square waves of different frequencies.

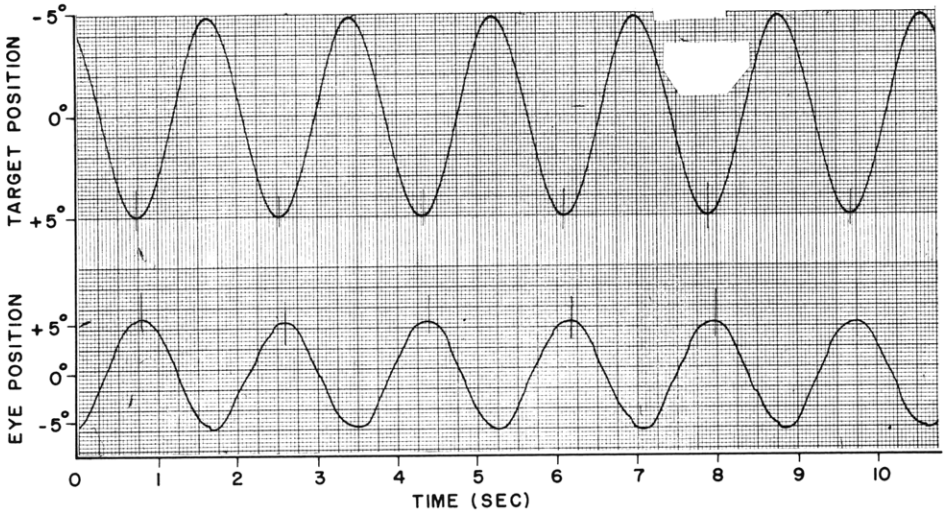


(a)

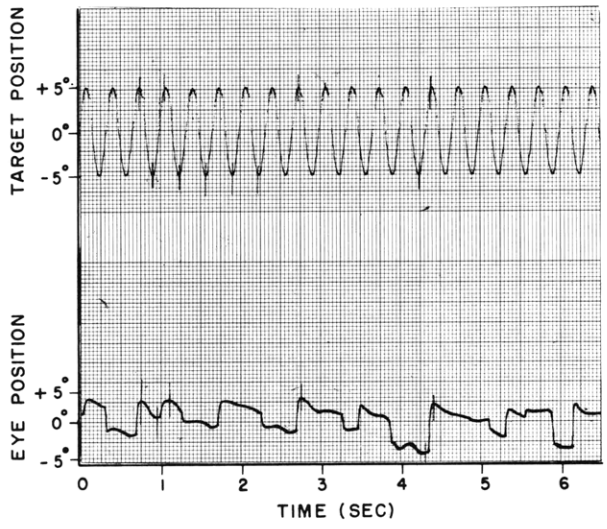


(b)

Fig. XV-30. Eye movement records for tracking of sinusoidal target motion: (a) 0.5 cps; (b) 3.0 cps.

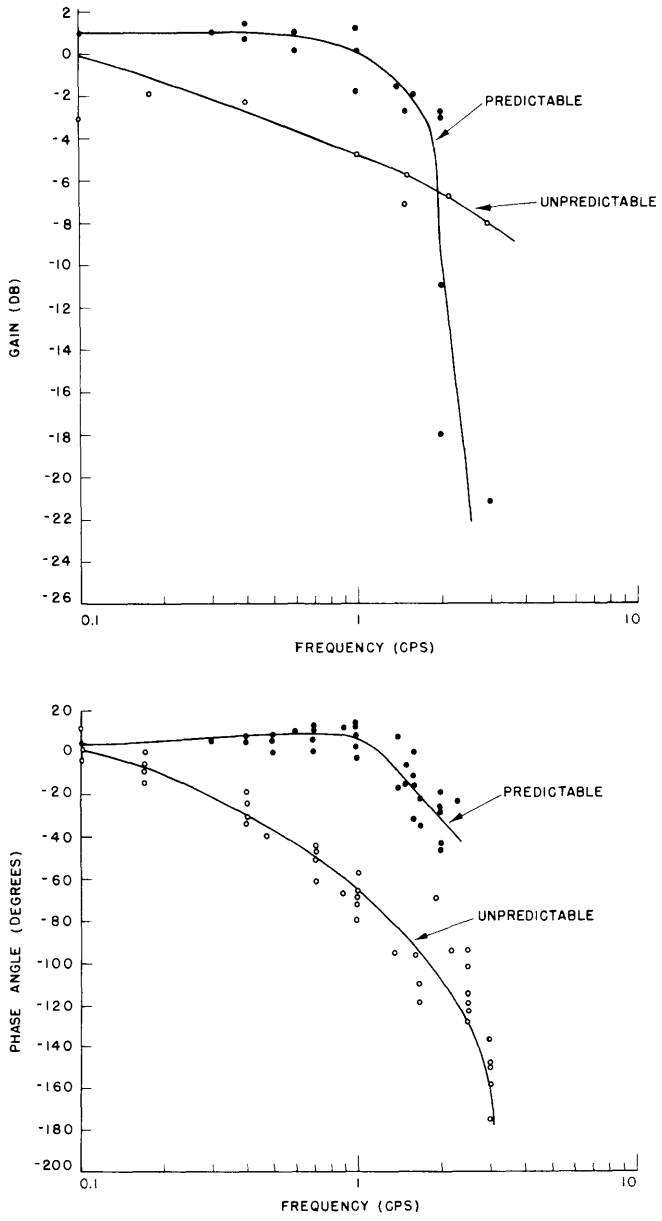


Fig. XV-31. Gain and phase relationships for continuous predictable and unpredictable target motions.

contrasted with the prediction and overprediction seen at intermediate rates.

b. Response to Single Sinusoids and Unpredictable Continuous Signals.

All of the preceding results pertain to the saccadic movements. When a single sinusoid is tracked, the "smooth pursuit" system plays an important role, as shown in Figs. XV-25 and XV-30. Here, after the target movement becomes accurately tracked, the occurrence of saccades is less obvious. The accuracy of the tracking is so high that the amount of phase lag and attenuation at low and intermediate frequencies is quite small (Fig. XV-30). At higher frequencies, as shown in Fig. XV-30b, the response becomes so erratic that it is difficult to identify the sinusoidal response. Saccadic movements are again prominent here. Data from steady-state experiments are summarized in the Bode plot of Fig. XV-31. Note the small phase advance or phase lag and, for those frequencies at which following can be said to exist (6), relatively constant gain.

In order to generate the continuous unpredictable target signal, from four to nine non-low-harmonically related sinusoids were summed by the RW-300 computer, and the resultant function appeared at the analog output of the computer. The eye-movement response was stored in the computer and then analyzed for the presence of those frequencies that made up the input. An example of such an experiment is shown in Fig. XV-32. It appears that smooth pursuit movements dominated the response to

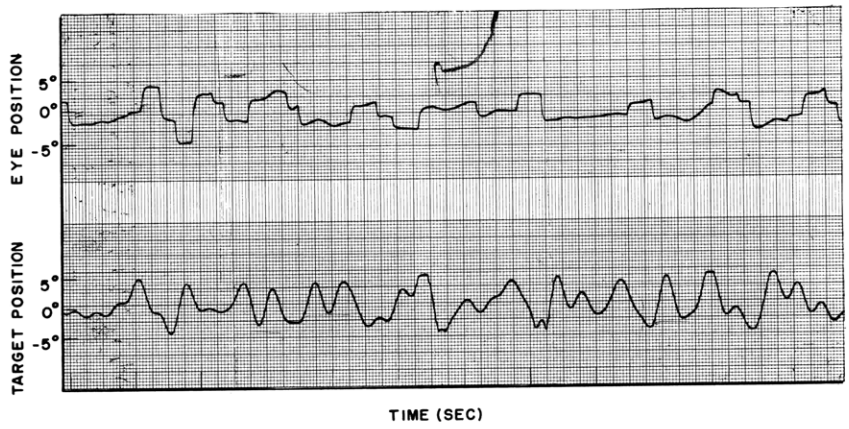


Fig. XV-32. A typical record of eye tracking of a sum of four sinusoids.

slowly varying portions of the continuous signal, while saccadic movements were more obvious at higher velocity portions.

Gain and phase data calculated by the computer as described previously (4) from a series of such experiments is shown in the Bode plot of Fig. XV-31. It is clear that there is a markedly increased phase lag with the unpredictable signal, as contrasted with the steady-state sinusoidal signal. This indicates that the prediction apparatus of

the brain is able to compensate for almost all of the inherent phase lag of the "neurological system"; however, compensation by the adaptive predictor for attenuation is less well defined in these initial experiments.

2. Discussion

The experimental data presented above clearly substantiate our main thesis, namely, the importance of controlling predictability of the input signal. If the aim is to describe and dissect the underlying biological servomechanisms, then it is necessary to negate the powerful predictive apparatus. Our experiments have been performed on only a few trained subjects and care must be taken not to ascribe too much significance to the detail of these records. It is our intent to study normal variability, physiological effects such as fatigue, and syndromes produced by pathological processes.

There are several other interesting facets of the control of eye movements which can be investigated with the current experimental apparatus. Among these, preliminary work has been done on the following experiments:

(a) Open-loop experiments. The visual feedback loop can be opened by using the eye position signal to drive the target position in such a manner as to maintain a fairly constant fixation error angle.

(b) Variable loop gain. By feeding back from the eye position signal to the target position command through a variable gain, the fixation angle will be reduced by an angle $K\theta$ for an eye rotation of $\theta$. The effects of this change on the stability and adaptivity of the system can be studied.

(c) Ramp inputs. When eye movements are recorded during fixation on a target moving with constant velocity the maximum pursuit velocity can be determined.

(d) Transient analyses. When an improvement in the eye-position monitoring system is completed, it is planned to examine in detail the transient response to step, ramp, and parabolic inputs of various magnitudes and under different initial conditions of eye position.

In order to supplement our references we are including a limited bibliography of interesting works on eye movements.

3. Summary

A simple instrument for measurement of eye movements has enabled us to show that changing the characteristics of the target-position signal has important effects on the nature of the biological servomechanism controlling the movement. In particular, there is an adaptive predictor that allows the system to overcome its innate delays upon exposure to a regular input pattern.

L. Stark, G. Vossius, L. R. Young

## References

1. R. Dodge and T. S. Cline, The angle velocity of eye movements, Psychol. Rev., No. 8, pp. 145-157, 1901.

2. C. Rashbass, Barbituato Nystagmus and the mechanisms of visual fixation, Nature 183, 897-898 (March 28, 1959).

3. L. Stark, L. M. Iida, and P. A. Willis, Dynamic characteristics of motor coordination, Quarterly Progress Report No. 60, Research Laboratory of Electronics, M. I. T., Jan. 15, 1961, pp. 231-233.

4. L. Stark, Y. Okabe, and others, Use of on-line digital computer for measurement of a neurological control system, Quarterly Progress Report No. 61, Research Laboratory of Electronics, M. I. T., April 15, 1961, pp. 219-222.

5. G. Vossius, Das System der Augenbewegung, Z. Biol. 112, No. 1 (1960).

6. A. Scunderhauf, Untersuchungen über die Regelund der Augenbewegung, Klinische Monatsblatter für Augenheilkunde, Vol. 136, No. 6, pp. 837-852, 1960.

## Bibliography

1. Dodge, R., and Cline, T. S.: The Angle Velocity of Eye Movements, Psychol. Rev. 8: 145, 1901.

2. Dodge, R.: Five Types of Eye Movements in the Horizontal Meridian Plane of the Field of Regard, Am. J. Physiol. 8: 307, 1903.

3. Judd, C. H.: Photographic Records of Convergence and Divergence, Psychol. Rev. (Monogr. Supp. 34) 8: 307, 1907.

4. Carmichael, L. and Dearborn, W. F.: Reading and Visual Fatigue (Houghton Mifflin Company, Boston, 1947).

5. Marg, E.: Development of Electro-Oculography: Standing Potential of the Eye in Registration of Eye Movements, A. M. A. Arch. Ophth. 45: 169, 1951.

6. Ratliff, F., and Riggs, L. A.: Involuntary Motions of the Eye During Monocular Fixation, J. Exper. Psychol. 40: 687, 1950.

7. Ditchburn, R. W., and Ginsborg, B. L.: Involuntary Eye Movements During Fixation, J. Physiol. 119: 1, 1953.

8. Adler, F. H., and Fliegelman, M.: Influence of Fixation on the Visual Acuity, Arch. Ophth. 12: 475, 1934.

9. Lord, M. P., and Wright, W. D.: Eye Movements During Monocular Fixation, Nature 162: 25, 1948.

10. Barlow, H. B.: Eye Movements During Fixation, J. Physiol. 116: 290, 1952.

11. Lorente de Nó, R.: Observations on Nystagmus, Acta oto-laryng. 21: 416, 1934.

12. Szentagothai, J.: Die Rolle der einzelnen Labyrinthrezeptoren bei der Orientation von Auge und Kopf im Raume, Kultura (Budapest), 1952.

13. Cooper, S., and Eccles, J. C.: Isometric Responses of Mammalian Muscles, J. Physiol. 69: 377, 1930.

14. McIntyre, A. K.: Quick Component of Nystagmus, J. Physiol. 97: 8, 1939.

(Bibliography continued on following page)

15. McCouch, G. P., and Adler, F. H.: Extraocular Reflexes, Am. J. Physiol. 100: 78, 1932.

16. Scunderhauf, A.: Untersuchungen über die Reglung der Augenbewegungen, Klinische Monatsblatter für Augenheilkunde, Vol. 136, No. 6, 1960.

17. Kris, C.: A Technique for Electrically Recording Eye Position, WADC Technical Report 58-660, Research Laboratory of Electronics, M. I. T., December 1958.

18. Cogan, D. G.: Neurology of the Ocular Muscles (Charles C. Thomas, Publishers, Springfield, Ill., 1948).

19. Riggs, L. A., and Ratliff, F.: Visual acuity and the normal tremor of the eyes, Science 114, 17 (1951).

20. Westheimer, G.: Mechanism of saccadic eye movements, Arch. Ophthalmol. 52, 710 (1954).

21. Ludwigh, E., and Miller, J. W.: Study of visual acuity during the ocular pursuit of moving test objects, I, J. Opt. Soc. Am. 48, 799 (1958).

22. Rashbass, C.: Barbiturate nystagmus and the mechanisms of visual fixation, Nature 183, 897 (1959).

23. Miller, J. W.: Study of visual acuity during the ocular pursuit of moving test objects, II, J. Opt. Soc. Am. 48, 803 (1958).

24. Shackel, B.: A note on mobile eye viewpoint recording, J. Opt. Soc. Am. (to be published).

25. Cornsweet, T. N.: New technique for the measurement of small eye movements, J. Opt. Soc. Am. 48, 808 (1958).

26. Mackworth, J. F., and Mackworth, N. H.: Eye fixations recorded on changing visual scenes on the television eye marker, J. Opt. Soc. Am. 48, 429 (1958).

27. Westheimer, G., Eye Movement Responses to a Horizontally Moving Visual Stimulus, A. M. A. Arch. Ophth. 52, 932 (Dec. 1954).

28. Hyde, J. E., and Davis, L. M., Extraocular proprioception in electrically induced eye movements, Am. J. Physiol. 198, 5 (May, 1960).

29. Hakas, P. and Kornhuber, H. H., Der vestibulare Nystagmus bei Grosshirnlasionen des Menschen, Arch. Psychiatrie und Zeitschrift f. d. ges. Neurologie 200, 19-35 (1959).

30. Lion, K. S., and Brockhurst, R. J., Study of Ocular Movements Under Stress, A. M. A. Arch. Ophthalmol. 46, 315 (September 1951).

31. Pasik, P., Pasik, T. and Krieger, H. P., Effects of Cerebral Lesions upon Optokinetic Nystagmus in Monkeys, J. Neurophysiol. 22, 297 (1959).

32. Pritchard, R. M., Heron, W., and Hebb, D. O., Visual perception approached by the method of stabilized images, Can. J. Psychol. 141, 2 (1960).

33. Rashbass, C., New Method for Recording Eye Movements, J. Opt. Soc. Am. 50, 642 (July 1960).

34. Rashbass, C., Barbiturate Nystagmus and the Mechanisms of Visual Fixation, Nature 183, 897 (March 28, 1959).

35. Richter, H. R., Principes de la Photo-Électro-Nystagmographie, Rev. Neurol. 94: 2: 1956, p. 138.

36. Jung, R. and Mittermaier, R., Zur objektiven Registriering und Analyse verschiedener Nystagmusformen, Arch. Ohren usw. Heilk. 146, 410 (1939).

(Bibliography continued on following page)

37. Warwick, R., Oculomotor Organisation, Ann. Roy. College of Surgeons of England 19, 36-52 (1956).

38. Vossius, G., Das System der Augenbewegung, Z. Biol. 112: 1 (1960).

39. Vossius, G. Der sogenannte, innere "Regelkreis der Willkurbewegung Kybernetik," 1: 1: 1961, p. 28.

40. Westheimer, G., A note on the response characteristics of the extraocular Muscle System, Bull. Math. Biophys., Vol. 20, 1958.

41. Smith, W. M., Eye Movement and Stimulus Movement; New Photoelectric Electromechanical System for Recording and Measuring Tracking Motions of the Eye, J. Opt. Soc. Am. 50: 3; 245 (March 1960).

42. Battersby, W. S., Bender, M. B., Wagman, I. H., and Karp, E., Neural Limitations of Visual Excitability: Alterations Produced by Cerebral Lesions, A. M. A. Arch. Neurol. 3: July 1960, p. 24.

## G. SIMULATION OF BIOLOGICAL CONTROL SYSTEMS

Our recent research work dealt with the development of BIOSIM, an IBM 709 digital computer program for simulation of dynamic systems of the type encountered in the study of biological control mechanisms.

In studying the behavior of biological control systems there arises a need for simulating their dynamic behavior. One way of doing this is to solve the differential equations governing their behavior on a general-purpose digital computer. An advantage of this approach is that it allows the simulation of general system nonlinearities. The chief disadvantage is the requirement of the knowledge of computer programming on the part of the user. To overcome this disadvantage, there was prepared a general computer program called "BIOSIM" for the simulation of a general class of dynamic systems from specifications of their block-diagram representation.

The simulated system is considered to be made up of summers, summer-integrators and transmissions among them. The input to the BIOSIM program is a deck of data cards specifying these transmissions. The program interprets these data cards, forms the difference equations approximating system behavior, and solves them to obtain system output as a function of time. Additional data cards specify the initial conditions, size of the time increment in the difference equations and the forms of output to be used. The program can generate printed output, plotted output on either a printer or a cathode-ray tube and punched output in a format appropriate for subsequent plotting on a Libroscope automatic plotter. This mode of operation does not necessitate recompilation of the program each time a new system is simulated and since the system is specified in terms of its block diagram, the program can be used even by those with no knowledge of programming.

The program BIOSIM solves the difference equations.

$$y_i(t+\Delta) = y_i(t) + \Delta \sum_k T_k(i, t, y_1(t), y_2(t), \ldots y_{N+M}(t)) \qquad i = 1, 2, \ldots N$$

$$y_i(t+\Delta) = \sum_k T_k(i, t+\Delta, y_1(t+\Delta), \ldots y_N(t+\Delta), y_{N+1}(t), \ldots y_{N+M}(t)) \qquad i = N+1, \ldots N+M$$

where $y_i$, $i = 1, 2 \ldots N$ are the outputs of the summer-integrators and are considered the state variables; $y_i$, $i = N+1, N+2, \ldots N+M$ are the auxiliary node variables, the outputs of summers. The simulation time is t, $\Delta$ is the time increment and $T_k(i, \ldots)$'s are the transmissions among summers and summer-integrators, which are the quantities specified by the data cards.

Standard forms of data cards allow the specification of the following transmissions.

$$T_k(i, t, y_j) = C_k y_j(t) \qquad T_k(i, t, y_j) = C_k |y_j(t)|$$

$$T_k(i, t, y_j) = C_k y_j(t - C'_k) \qquad T_k(i, t, y_j) = C_k \log_e (C'_k y_j(t))$$

$$T_k(i, t, y_{j_1}, y_{j_2}) = C_k y_{j_1}(t)\, y_{j_2}(t) \qquad T_k(i, t, y_j) = C_k \exp (C'_k y_j(t))$$

$$T_k(i, t, y_{j_1}, y_{j_2}) = C_k y_{j_1}(t)/y_{j_2}(t) \qquad T_k(i, t, y_j) = C_k \exp (C'_k + C''_k / y_j(t))$$

$$T_k(i, t, y_j) = \begin{cases} C_k \beta_k & \text{if } C'_k y_j(t) \geq \beta_k \\ C_k C'_k y_j(t) & \text{otherwise} \\ C_k \alpha_k & \text{if } C'_k y_j(t) \leq \alpha_k \end{cases}$$

The current work attempts to incorporate in the simulator a compiler phase that would allow the specification of transmissions by FORTRAN-like expressions without going through a FORTRAN compiler. This feature will further simplify the use of the simulator.

Rather than rely on the FORTRAN compiler, a new interpreter-compiler was written that is so fast that a new compilation can be made each time the program is run. The absence of dc loops and variable subscripts, as well as the fact that neither punched nor printed compiler output is needed, makes the compilation approximately 10 times faster than FORTRAN.

The compiler itself has been completed but has not yet been incorporated in the simulator. Its salient feature is its multiscan structure. An interpretation assembly scan comes first in which operation symbols are encoded, decimal numbers are converted to binary, and the binary equivalents as well as variables are assigned storage locations. The operation codes and variable addresses are stored in an interpreter list. In the compilation the hierarchies of operations are compiled in succession scanning from the right. Within each pair of enclosing parentheses a scan from left compiles in the compiler

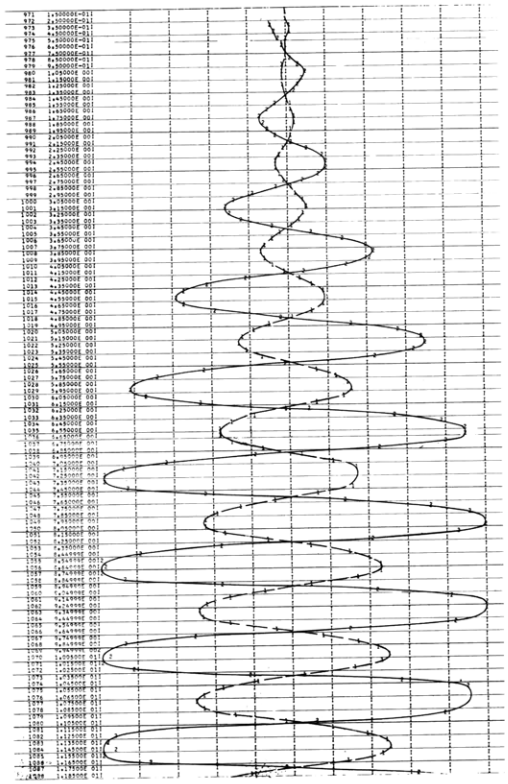

Fig. XV-33. Time-function plot of two variables in a closed-loop pupil-environmental clamp system that is on the border line of instability oscillations. The input is computation noise. The simulation was run on the IBM 709 computer of the Computation Center, M. I. T.

list multiplications, divisions and storage of partial answers in auxiliary storage. The interpreter list entries, which were compiled, are erased and replaced by addresses of partial answers. The next scan from the right compiler additions and subtractions erases the compiled entries in the interpreter list. On meeting an "=" sign the compiled program stores the answer in the address of the left-hand side of the expression. Upon meeting a comma an element of a function calling sequence is compiled. Upon meeting a left parenthesis, if what is to its left is a function name, the program compiles a transfer to this function, otherwise a partial answer is stored, its address replaces the bracketed expression, and the program continues scanning left into the next hierarchy of operations.

This compiler does not include error diagnosing and optimizing programs. These may be added in the future.

The simulator has already been used in the study of the Parke oscillations of the human pupil system.

Figure XV-33 shows the system developing high gain and instability oscillations, which are a model for those described in Quarterly Progress Report No. 61 (pages 219-222).

V. W. Kipiniak